がんの放射線治療がよくわかる本

第1章 放射線治療とは

第2章 より強力・安全になった放射線治療の最前線

第3章 がんの種類別／最新の放射線治療

第4章 放射線治療の副作用とその対処法

第5章 Q&A 安心して治療を受けるために

Geometrical differences in target volumes between slow CT and 4D CT imaging in stereotactic body radiotherapy for lung tumors in the upper and middle lobe

Mitsuhiro Nakamura, Yuichiro Narita,[a] Yukinori Matsuo, and Masaru Narabayashi
Department of Radiation Oncology and Image-applied Therapy, Graduate School of Medicine, Kyoto University, Kyoto 606-8507, Japan

Manabu Nakata and Shinsuke Yano
Clinical Radiology Service Division, Kyoto University Hospital, Kyoto 606-8507, Japan

Yuki Miyabe, Kiyotomo Matsugi, Akira Sawada, Yoshiki Norihisa, and Takashi Mizowaki
Department of Radiation Oncology and Image-applied Therapy, Graduate School of Medicine, Kyoto University, Kyoto 606-8507, Japan

Yasushi Nagata
Division of Radiation Oncology, Hiroshima University Hospital, Hiroshima 734-0037, Japan

Masahiro Hiraoka
Department of Radiation Oncology and Image-applied Therapy, Graduate School of Medicine, Kyoto University, Kyoto 606-8507, Japan

(Received 19 March 2008; revised 7 July 2008; accepted for publication 16 July 2008; published 19 August 2008)

Since stereotactic body radiotherapy (SBRT) was started for patients with lung tumor in 1998 in our institution, x-ray fluoroscopic examination and slow computed tomography (CT) scan with a rotation time of 4 s have been routinely applied to determine target volumes. When lung tumor motion observed with x-ray fluoroscopy is larger than 8 mm, diaphragm control (DC) is used to reduce tumor motion during respiration. After the installation of a four-dimensional (4D) CT scanner in 2006, 4D CT images have been supplementarily acquired to determine target volumes. It was found that target volumes based on slow CT images were substantially different from those on 4D CT images, even for patients with lung tumor motion no larger than 8 mm. Although slow CT scan might be expected to fare well for lung tumors with motion range of 8 mm or less, the potential limitations of slow CT scan are unknown. The purpose of this study was to evaluate the geometrical differences in target volumes between slow CT and 4D CT imaging for lung tumors with motion range no larger than 8 mm in the upper and middle lobe. Of the patients who underwent SBRT between October 2006 and April 2008, 32 patients who had lung tumor with motion range no larger than 8 mm and did not need to use DC were enrolled in this study. Slow CT and 4D CT images were acquired under free breathing for each patient. Target volumes were manually delineated on slow CT images ($TV_{slow\ CT}$). Gross tumor volumes were also delineated on each of the 4D CT volumes and their union ($TV_{4D\ CT}$) was constructed. Volumetric and statistical analyses were performed for each patient. The mean ± standard deviation (S.D.) of $TV_{slow\ CT}/TV_{4D\ CT}$ was 0.75 ± 0.17 (range, 0.38–1.10). The difference between sizes of $TV_{slow\ CT}$ and $TV_{4D\ CT}$ was not statistically significant ($P=0.096$). A mean of 8% volume of $TV_{slow\ CT}$ was not encompassed in $TV_{4D\ CT}$ (mean ± S.D. $= 0.92 \pm 0.07$). The patients were separated into two groups to test whether the quality of target delineation on slow CT scans depends on respiratory periods below or above the CT rotation time of 4 s. No significant difference was observed between these groups ($P=0.229$). Even lung tumors with motion range no larger than 8 mm might not be accurately depicted on slow CT images. When only a single slow CT scan was used for lung tumors with motion range of 8 mm or less, 95% confidence values for additional margins for $TV_{slow\ CT}$ to encompass $TV_{4D\ CT}$ were 4.0, 5.4, 4.9, 5.1, 1.8, and 1.7 mm for lateral, medial, ventral, dorsal, cranial, and caudal directions, respectively.
[DOI: 10.1118/1.2968096]

Key words: 4D CT, slow CT, respiratory motion, margin, lung cancer

I. INTRODUCTION

The local control rate of conventional radiotherapy is not satisfactory for lung cancer, even in stage I cases.[1,2] However, since the introduction of stereotactic body radiotherapy (SBRT), higher local control rates comparable to those with surgery have been reported.[3–7] In recent years, guidelines for SBRT have been developed and written collaboratively by the American Society of Therapeutic Radiology and Oncol-

ogy and the American College of Radiology.[8] SBRT is increasingly becoming an important treatment option for stage I lung cancer.

SBRT allows high-dose areas limited to a target volume with a high degree of precision within the body and reduces doses delivered to other areas such as organs at risk. Therefore, target delineation is more crucial in treatment planning of SBRT. While there is an increasing use of multiple imaging modalities, current treatment planning is primarily based on computed tomography (CT). It has been recognized that severe motion artifacts, including axial slices being shuffled out of order and organs being imaged as distinct parts, can sometimes be introduced if organ motion is present during standard CT scan under free breathing.[9–11] Such motion artifacts may give an inaccurate representation of the shape, volume, and position of normal organs and target volumes, and lead to crucial delineation error in treatment planning. Three CT acquisition methods are commonly used to visualize the entire range of respiratory tumor motion on CT images, namely inhale and exhale breath-hold CT scan,[12–14] slow CT scan,[15–17] and four-dimensional (4D) CT scan.[18–22]

In our institution, SBRT was started in 1998 for patients with lung tumor. The eligibility criteria of SBRT for lung tumor in our institution are as follows: (1) tumor diameter is no larger than 4 cm, (2) tumor is located peripherally, and (3) one or two tumors in metastasis cases. X-ray fluoroscopic examination and slow CT scan with a rotation time of 4 s have been routinely applied to determine target volumes. When lung tumor motion observed with x-ray fluoroscopy is larger than 8 mm, a small abdominal pressure plate, called "diaphragm control (DC)," is applied to reduce tumor motion.[23] Additionally, x-ray fluoroscopy is used to determine whether the target volume visualized on slow CT images is sufficiently large to encompass tumor motion. When the target volume on slow CT images is found to be insufficient, we manually correct the target volume based on x-ray fluoroscopy evaluation. Since a four-slice CT scanner which allows 4D CT scan was installed in 2006, 4D CT images have been supplementarily utilized to determine target volumes. We found that target volumes based on slow CT images were substantially different from those based on 4D CT images, even for patients with lung tumor motion no larger than 8 mm. The observed differences need to be quantitatively reflected in treatment planning.

Some researchers compared the difference in target volumes between different CT scan techniques for patients with lung tumors.[16,20,24,25] van Sörnsen de Koste *et al.* and Seki *et al.* showed the effectiveness of the combined use of slow CT and helical CT in the delineation of internal target volume.[16,24] Underberg *et al.* reported that a single 4D CT scan can replace six rapid helical CT scans in defining individualized target volumes for stage I non-small cell lung cancer.[20] Bradley *et al.* compared helical CT, maximum intensity projection, and averaged intensity 4D CT images to determine the best CT-based volume definition method for encompassing tumor motion within the planning target volume (PTV) for SBRT in stage I lung cancer.[25] However, the comparison of the target volumes based on slow CT scan with those based on 4D CT scan has not yet been reported. The potential limitations of slow CT scan are also unknown, although slow CT scan might be expected to fare well for lung tumors with motion range of 8 mm or less. The purpose of this study was to evaluate the geometrical differences in target volumes between slow CT and 4D CT imaging for lung tumors with motion range no larger than 8 mm in the upper and middle lobe.

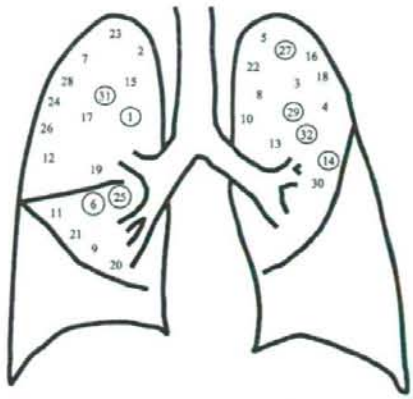

FIG. 1. Diagram of lung tumor location for each patient. Numbers represent case numbers. Lung tumors were peripherally located in the right upper lobe (12 patients), in the right middle lobe (6 patients), and in the left upper lobe (14 patients). Data of the circled numbers are shown in Tables I and II.

II. MATERIALS AND METHODS

II.A. Patients

Of the patients who underwent SBRT between October 2006 and April 2008, 32 patients who had lung tumor with motion range no larger than 8 mm and did not need to use DC after x-ray fluoroscopic evaluation were enrolled in this study. If DC was required to limit respiratory motion, reliable motion signals could not be acquired for 4D CT data acquisition and therefore these patients were excluded from this study. Twenty-three men and nine women with a median age of 74 years (range, 56–87 years) were included. Lung tumors were located in the right upper lobe (12 patients), in the right middle lobe (6 patients), and in the left upper lobe (14 patients) (Fig. 1). Written informed consent for SBRT was obtained from each patient before treatment planning.

II.B. X-ray fluoroscopic evaluation and CT data acquisition

Before CT data acquisition, the patient was fixed in a stereotactic body frame (SBF) (Elekta Corp., Stockholm, Sweden) with their arms raised using a vacuum pillow.[23,26] The patient was asked to breathe regularly and quietly by radiological technicians. Respiratory tumor motion was then observed with an x-ray simulator (Acuity; Varian Medical

Systems, Palo Alto, CA) from orthogonal directions. DC was applied to reduce lung tumor motion when it was larger than 8 mm.[23]

After x-ray fluoroscopic evaluation, the patient immobilized with SBF was placed on the couch of a CT scanner (LightSpeed RT; General Electric Medical Systems, Waukesha, WI). First, slow CT scan was routinely performed. CT slices were sequentially acquired from the lower neck to the upper abdomen in axial mode. The CT slice thickness and rotation time were 1.25 mm and 4 s around the tumor and 2.5 mm and 1 s in the other areas, respectively. Immediately after the slow CT scan, 4D CT data were acquired only around an area including the lung tumor using the Real-time Positioning Management (RPM) system (Varian) in axial cine mode.[18–22] Cine duration time of the scan at each couch position was set to 6 or 7.5 s, which was more than the maximum observed respiratory period. Cine interval between images was 0.5 s. With these settings, we usually obtain approximately 12–15 images per couch position. To prevent marker vibration resulting from couch movement, interscan delay was set to longer than 2 s. CT data were reconstructed in a field of view of 520 mm on a 512×512 grid for both CT scans. The RPM system illuminated and tracked an infrared reflective marker placed on the patient's abdomen. RPM software calculated the respiratory phase at each instant in time based on modeling the abdominal motion amplitude. Motion phases were assigned for each respiratory phase in percent values, end-inhalation corresponding to 0% and end-exhalation to 50%. After 4D CT scan, all 4D CT slices and respiratory motion data were transferred to an Advantage 4D workstation (GE), and Advantage 4D software retrospectively sorted the images into eight respiratory phase bins.

II.C. Target volume definition

All CT datasets were imported into a commercial three-dimensional radiation planning system (Eclipse 7.3.10; Varian), and thereafter slow CT images and 4D CT images were superimposed using the same coordinate origin that they shared. Alignment of bony structures was reviewed by one medical physicist (M.N.) on subtraction images to check the patient's movement between slow CT scan and 4D CT scan. Target volumes were delineated on the Eclipse using lung CT window setting [window width: 2000 Hounsfield units (HU) and window level: -700 HU]. To eliminate inter-observer variations,[27–29] target volumes were manually contoured by the same medical physicist (M.N.) on slow CT scan images as well as 4D CT images. All contours were reviewed by one experienced radiation oncologist (Y.M.). The definitions of all different target volumes generated were as follows.

- $GTV_{T\%}$: Gross tumor volume (GTV) delineated on T% phase of 4D CT images. Each $GTV_{T\%}$ was defined without reference to previously contoured GTVs.
- $TV_{4D\ CT}$: Target volume derived from contouring GTVs on all eight phases of the 4D CT. $TV_{4D\ CT}$ was defined as follows:

$$TV_{4D\ CT} = GTV_{0\%} \cup GTV_{12\%} \cup \cdots \cup GTV_{87\%}.$$

- $TV_{slow\ CT}$: Target volume derived from slow CT scan. $TV_{slow\ CT}$ included a blurred area surrounding the tumor. The area indicated respiratory motion.
- TV_{COM}: Target volume defined as an overlapping volume between $TV_{slow\ CT}$ and $TV_{4D\ CT}$. TV_{COM} was defined as follows:

$$TV_{COM} = TV_{slow\ CT} \cap TV_{4D\ CT}.$$

II.D. Analysis

From 4D CT datasets, volumetric variations in GTVs for each patient were analyzed. The coefficient of variation (C.V.) was employed to evaluate variations in the GTV size because of motion artifacts and tumor deformation during respiration.[22] Intrafractional motion range of the GTVs was also measured in the right-left (RL), anterior-posterior (AP), and cranial-caudal (CC) directions.

The size and centroid shift between $TV_{slow\ CT}$ and $TV_{4D\ CT}$ were compared for all patients. When $TV_{slow\ CT}$ is fully covered by $TV_{4D\ CT}$, TV_{COM} is equal to $TV_{slow\ CT}$. In order to test whether slow CT scan with a rotation time of

TABLE I. Volumetric variations and motion range of GTVs as well as the averaged breathing period for patients with 3D GTV centroid motion range larger than 4.4 mm corresponding to the 75th percentile. *Abbreviations:* GTV=gross tumor volume; Avg.=average; S.D.=standard deviation; C.V.=coefficient of variation; RL=right-left; AP=anterior-posterior; CC=cranial-caudal; $3D=\sqrt{RL^2+AP^2+CC^2}$.

	GTV			Motion range (mm)				Averaged breathing period (s)
Case	Avg. (ml)	S.D. (ml)	C.V. (%)	RL	AP	CC	3D	
1	2.11	0.13	6.08	1.3	3.6	5.8	6.9	5.63
6	1.45	0.13	8.99	3.9	4.5	1.4	6.1	4.27
14	3.99	0.27	6.77	0.8	4.2	4.9	6.5	4.38
25	0.56	0.01	2.32	3.0	1.5	7.1	7.9	4.80
27	3.09	0.23	7.44	1.0	2.4	5.5	6.1	3.54
29	4.49	0.26	5.79	1.0	3.2	2.9	4.4	3.66
31	11.73	0.76	6.48	1.9	2.9	2.7	4.4	5.55
32	1.33	0.08	6.02	1.4	3.3	4.1	5.4	3.27

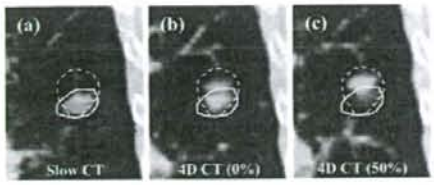

FIG. 2. Coronal images for case 32. Left: slow CT scan. Middle: 0% phase of 4D CT scan. Right: 50% phase of 4D CT scan. Outlines of $TV_{slow\ CT}$ (solid line) and $TV_{4D\ CT}$ (broken line) were overlaid. Additional margins to encompass $TV_{4D\ CT}$ was 0.0, 3.4, 0.6, 5.7, 7.5, and 0.0 mm for lateral, medial, ventral, dorsal, cranial, and caudal directions, respectively.

4 s can capture the motion of a lung tumor in less than 4 s ("<4 sec"), the patients were categorized into a group with a breathing period of "<4 sec" and a group with that of 4 s or longer ("≥4 sec"). The ratio of $TV_{slow\ CT}$ to $TV_{4D\ CT}$ ($TV_{slow\ CT}/TV_{4D\ CT}$) for the two groups was compared.

Maximum distances for lateral-medial, ventral-dorsal, and cranial-caudal directions between $TV_{slow\ CT}$ and $TV_{4D\ CT}$ were measured on anterior-posterior and lateral beam's-eye-view projections. The distances were used to determine the additional margins needed for $TV_{slow\ CT}$ to ensure complete coverage of $TV_{4D\ CT}$ on the Eclipse.

The one-sided Wilcoxon test was performed for statistical analyses. Values of $P<0.05$ were regarded as significant.

III. RESULTS

III.A. 4D CT analysis

The C.V. in GTV volumes ranged from 0.54% to 8.99% with a mean of 3.92% for all cases. The mean ± standard deviation (S.D.) motion ranges were 1.0 ± 0.8, 1.8 ± 1.1, and 2.3 ± 1.7 mm in the RL, AP, and CC directions, respectively. The mean ± S.D. of 3D GTV centroid motion range was 3.3 ± 1.9 mm (range, 0.5–7.9 mm). The breathing period in patients ranged from 2.40 to 6.80 s with a mean ± S.D. of 4.19 ± 0.98 s. Table I shows volumetric variations and motion range of GTVs as well as the averaged breathing period for the patients with 3D GTV centroid motion range larger than 4.4 mm corresponding to the 75th percentile. The maximum C.V. is included in Table I.

III.B. Target volume analysis

Misalignment of bony structures that greatly affected the subsequent results was not seen in any cases. Although the patients did not move between slow CT scan and 4D CT scan, the size and centroid of $TV_{slow\ CT}$ differed from those of $TV_{4D\ CT}$ (Fig. 2). The mean ± S.D. sizes of $TV_{slow\ CT}$ and $TV_{4D\ CT}$ were 6.41 ± 5.70 ml (range, 0.26–24.35 ml) and 8.02 ± 6.21 ml (range, 0.35–24.66 ml), respectively. The mean ± S.D. of $TV_{slow\ CT}/TV_{4D\ CT}$ was 0.75 ± 0.17 (range, 0.38–1.10). The size of $TV_{slow\ CT}$ was smaller than that of $TV_{4D\ CT}$ except in case 4. The difference between the sizes of $TV_{slow\ CT}$ and $TV_{4D\ CT}$ was not statistically significant ($P=0.096$). The mean ± S.D. of centroid shift between $TV_{slow\ CT}$ and $TV_{4D\ CT}$ was 1.5 ± 1.0 mm (range, 0.4–4.8 mm). The mean ± S.D. of $TV_{COM}/TV_{slow\ CT}$ was 0.92 ± 0.07. Table II summarizes the results of $TV_{slow\ CT}$, $TV_{4D\ CT}$, and TV_{COM} for the same patients as in Table I. The minimum $TV_{slow\ CT}/TV_{4D\ CT}$ and the maximum centroid shift are included in Table II. The mean ± S.D. of the breathing periods for the groups of "<4 sec" (14 patients, 43.75%) and "≥4 sec" (18 patients, 56.25%) were 3.32 ± 0.45 s and 4.87 ± 0.69 s, respectively. By comparing $TV_{slow\ CT}/TV_{4D\ CT}$ between the group of "<4 sec" and that of "≥4 sec," the quartile deviation of $TV_{slow\ CT}/TV_{4D\ CT}$ for the group of "<4 sec" was smaller than for the group of "≥4 sec" (Fig. 3). No significant difference was observed between these groups ($P=0.229$).

III.C. Estimation of additional margins

The margins required for $TV_{slow\ CT}$ to encompass $TV_{4D\ CT}$ are shown in Fig. 4. A large variation of margins in each direction was observed among patients. Fifteen patients did not require an additional margin in either the cranial or caudal direction. When only a single slow CT scan was used for treatment planning, 95% confidence values for the addi-

TABLE II. Summary table of $TV_{slow\ CT}$, $TV_{4D\ CT}$, and TV_{COM} for the same patients as in Table I. *Abbreviations:* S.D.=standard deviation; RL=right-left; AP=anterior-posterior; CC=cranial-caudal; $3D=\sqrt{RL^2+AP^2+CC^2}$. *Note:* For centroid shift, a positive value indicates that the centroid of $TV_{4D\ CT}$ is larger than that of $TV_{slow\ CT}$.

						Centroid shift (mm)			
Case	$TV_{slow\ CT}$ (ml)	$TV_{4D\ CT}$ (ml)	TV_{COM} (ml)	$TV_{slow\ CT}/TV_{4D\ CT}$	$TV_{COM}/TV_{slow\ CT}$	RL	AP	CC	3D
1	1.70	4.38	1.68	0.39	0.99	1.1	0.5	0.9	1.5
6	2.20	2.68	1.82	0.82	0.83	1.0	−0.8	1.6	2.0
14	4.10	6.47	3.62	0.63	0.88	−1.2	3.0	1.4	3.5
25	0.49	1.29	0.48	0.38	0.98	−1.1	−1.0	−0.2	1.5
27	4.46	5.46	3.98	0.82	0.89	−0.2	1.8	−0.4	1.9
29	7.49	8.88	6.44	0.84	0.86	−0.2	2.3	−1.3	2.6
31	12.02	18.58	11.67	0.65	0.97	−0.5	0.6	−1.6	1.8
32	1.04	2.45	0.8	0.42	0.77	−0.8	1.3	4.5	4.8

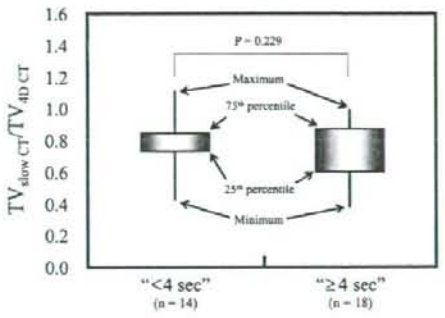

FIG. 3. Comparison of $TV_{slow\ CT}/TV_{4D\ CT}$ for the group of "<4 sec" with that for the group of "≥4 sec" using boxplot. No significant difference was observed between these groups (P=0.229).

tional margin to encompass $TV_{4D\ CT}$ were 4.0, 5.4, 4.9, 5.1, 1.8, and 1.7 mm for lateral, medial, ventral, dorsal, cranial, and caudal directions, respectively.

IV. DISCUSSION

In general, 4D CT data are analyzed to determine the mean tumor position and tumor range of motion.[18,19,21,22] However, data reliability is affected in the presence of motion artifacts. Rietzel *et al.* indicated that large deviations in GTV volume were seen in respiratory phases, especially near mid-exhalation and mid-inhalation because of the maximum velocity of the GTV.[21,22] They employed a C.V. as an index to compare variations in GTV sizes between patients who had significantly different mean GTV sizes, and showed the mean C.V. of 8.2% for the lung tumor in the upper lobe. Residual motion artifacts not only cause a C.V. to be larger, but also incorrectly characterize the geometric shape and extent of the organ. If the target volume is properly delineated without any motion artifacts, a C.V. is ideally zero, but this is uncommon because of motion artifacts and tumor deformation. In this study, evident motion artifacts affecting our results were not observed for any patients in movie-loops viewed in sagittal and coronal reconstructions of the 4D CT. In addition, our mean ± S.D. of the C.V. was 3.92 ± 2.39%, which was relatively lower than the results of Rietzel *et al.*[22] From the results of 4D CT analysis, we judged that the volume and centroid of $TV_{4D\ CT}$ could be reliable. While this study presents data for tumors in the upper and middle lung with motion of 8 mm or less only, other investigators reported lung tumor motion without such selection.[30,31] Given this limitation, our results are valid for tumors in the upper and middle lung with motion of 8 mm or less only.

Seppenwoolde *et al.* and Chen *et al.* reported that the breathing period in patients with lung cancer was within 4 s for most cases.[30,32] The mean ± S.D. of the breathing period was 4.19 ± 0.98 s, and the breathing period was more than 4 s for 18 patients in this study. van Sörnsen de Koste *et al.* described that most lung tumor mobility with a breathing period of less than 4 s could be captured with a slow CT scan with a rotation time of 4 s.[16] From our results of $TV_{slow\ CT}/TV_{4D\ CT}$ analysis, $TV_{slow\ CT}$ was smaller than $TV_{4D\ CT}$, except in case 4, even if the breathing period was less than 4 s. This means that the slow CT scan did not totally capture the motion of the lung tumor with a period of less than 4 s. For example, an additional margin of 7.5 mm was required in the cranial direction for case 32 with an averaged breathing period of 3.27 s. As shown in Fig. 2, his breathing might intermittently cease in the inhalation phase during slow CT scan. Most patients vary their respiratory pattern in frequency, amplitude, and waveform shape.[30] Therefore, the motion pattern of lung tumors during CT scan might be more important in differentiating $TV_{slow\ CT}$ and $TV_{4D\ CT}$ than the breathing period. Patients should be encouraged to perform reproducible and regular respiration during CT data acquisition.

Lagerwaard *et al.* examined how much margin was needed to ensure target volumes with multiple CT scans for lung tumors in the upper and middle lobe.[15] They concluded that the addition of a symmetrical 3D margin of 5 mm to a single slow CT ensured coverage of the "optimal" target volume derived from summation of the target volumes from multiple slow CT scans when only a single slow CT scan was used for treatment planning. Our results are nearly in agreement with the conclusion in regard to the transaxial plane, except in the CC direction. Our CT slice thickness of 1.25 mm is thinner than in their study where the CT slice thickness was 4 mm.[15] Thin-slice CT improves longitudinal resolution and enhances tumor detectability in the CC direction. High longitudinal resolution can decrease partial volume effects and lead to accurate delineation in the CC direction. Thus, thinner CT slices would make it possible to reduce additional margins in the CC direction. Despite the difference in CT slice thickness between slow CT scan and 4D CT scan, the additional margins were smaller in the CC direction than in other directions. This indicates that our results might not be biased by these differences.

Since 1998 we have performed SBRT for more than 250 patients with lung tumor. Our target determination protocol in SBRT planning is traditionally based on the slow CT scan protocol, which includes x-ray fluoroscopic examination to help define the target volume.[7,23,33] Currently, 4D CT images are also utilized to confirm the target volume. We showed that $TV_{slow\ CT}$ was smaller than $TV_{4D\ CT}$ for most cases. When determining target volumes in clinical practice, however, lung tumor motion observed with x-ray fluoroscopy is considered. Therefore, the clinically determined target volume is usually larger than the $TV_{slow\ CT}$ of this study. In addition, both setup margin and the margin between the PTV and the field edge are 5 mm in the Japan Clinical Oncology Group (http://www.jcog.jp/) number 0403 protocol. Nagata *et al.* reported that our local control rate of SBRT was 97% for 48 Gy in four fractions with a median follow-up of 30 months,[7] which is comparable to other results.[3–6] Considering our clinical results, our traditional protocol of target determination might be clinically acceptable.

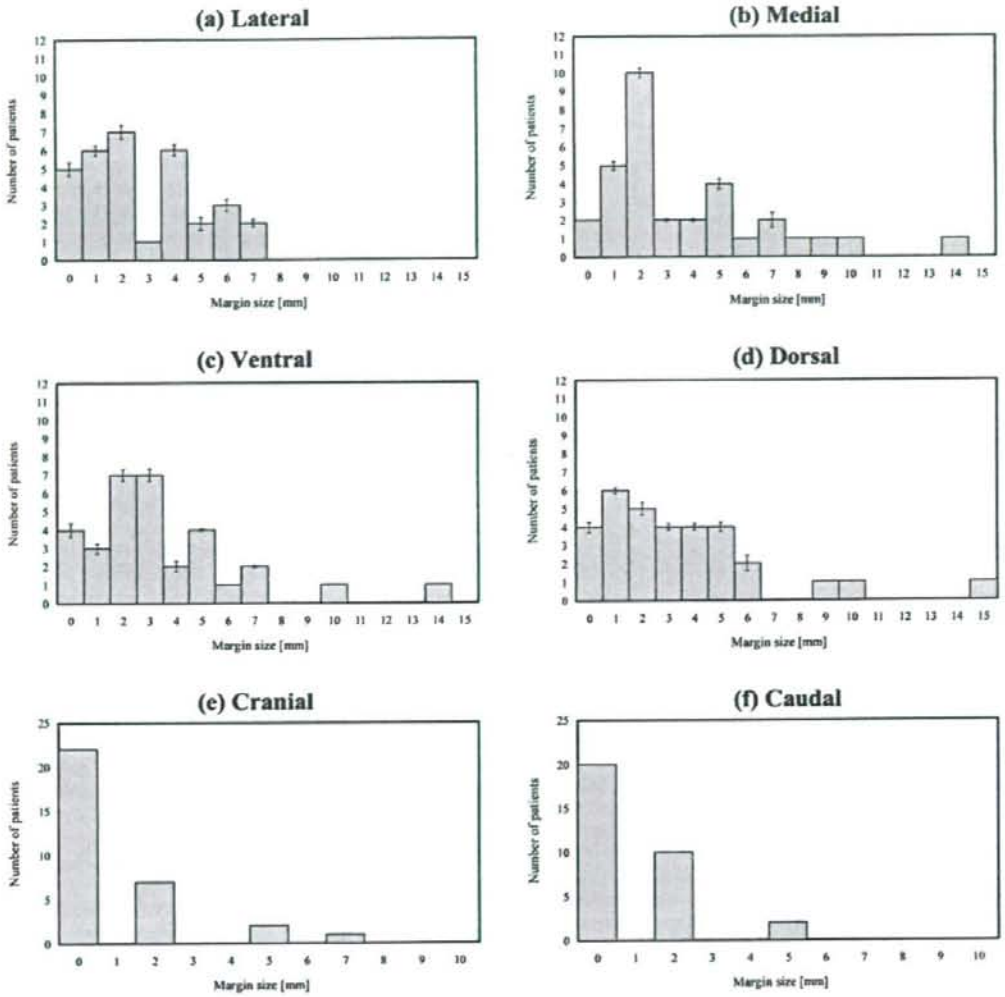

FIG. 4. Histograms of additional margins to the $TV_{slow\ CT}$ required for full coverage of $TV_{4D\ CT}$ for (a) lateral, (b) medial, (c) ventral, (d) dorsal, (e) cranial, and (f) caudal directions.

V. CONCLUSIONS

By comparing the target volume defined on slow CT images ($TV_{slow\ CT}$) with that defined on 4D CT images ($TV_{4D\ CT}$) for 32 lung tumors with motion range no larger than 8 mm in the upper and middle lobe, we evaluated geometrical differences between $TV_{slow\ CT}$ and $TV_{4D\ CT}$ and examined the additional margins needed for $TV_{slow\ CT}$ to ensure complete coverage of $TV_{4D\ CT}$. Our results revealed that a mean of 92% volume of $TV_{slow\ CT}$ was encompassed in $TV_{4D\ CT}$, and that additional margins to generate the target volume corresponding to $TV_{4D\ CT}$ are required even for lung tumors with motion range of 8 mm or less when only a single slow CT scan was used in treatment planning of SBRT.

ACKNOWLEDGMENTS

This study was conducted as part of the national project entitled "Fundamental investigation to develop a high-precision four-dimensional radiation therapy system," supported by the New Energy and Industrial Technology Development Organization (NEDO), and partly supported by a

Grant-in-Aid for Scientific Research from the Japan Society for the Promotion of Science (Grant No. 20229009).

[a]Author to whom correspondence should be addressed: Graduate School of Medicine, Kyoto University, Kyoto, 54 Kawara-cho, Shogoin, Sakyo-ku, Kyoto, 606-8507, Japan. Electronic mail: ynrt@kuhp.kyoto-u.ac.jp; Tel: (+81)-75-751-3762, Fax: (+81)-75-771-9749.

[1]F. J. Lagerwaard, S. Senan, J. P. van Meerbeeck, and W. J. Graveland, "Has 3-D conformal radiotherapy (3D CRT) improved the local tumour control for stage I non-small cell lung cancer?," Radiother. Oncol. **63**, 151–157 (2002).

[2]X. Qiao, O. Tullgren, I. Lax, F. Sirzén, and R. Lewensohn, "The role of radiotherapy in treatment of stage I non-small cell lung cancer," Lung Cancer **41**, 1–11 (2003).

[3]M. Uematsu, A. Shioda, A. Suda, T. Fukui, Y. Ozeki, Y. Hama, J. R. Wong, and S. Kusano, "Computed tomography-guided frameless stereotactic radiotherapy for stage I non-small cell lung cancer: A 5-year experience," Int. J. Radiat. Oncol., Biol., Phys. **51**, 666–670 (2001).

[4]R. Onimaru, H. Shirato, S. Shimizu, K. Kitamura, B. Xu, S. Fukumoto, T. C. Chang, K. Fujita, M. Oita, K. Miyasaka, M. Nishimura, and H. Dosaka-Akita, "Tolerance of organs at risk in small-volume, hypofractionated, image-guided radiotherapy for primary and metastatic lung cancers," Int. J. Radiat. Oncol., Biol., Phys. **56**, 126–135 (2003).

[5]R. Timmerman, L. Papiez, R. McGarry, L. Likes, C. DesRosiers, S. Frost, and M. Williams, "Extracranial stereotactic radioablation: results of a phase I study in medically inoperable stage I non-small cell lung cancer," Chest **124**, 1946–1955 (2003).

[6]J. Wulf, U. Haedinger, U. Oppitz, W. Thiele, G. Mueller, and M. Flentje, "Stereotactic radiotherapy for primary lung cancer and pulmonary metastases: A noninvasive treatment approach in medically inoperable patients," Int. J. Radiat. Oncol., Biol., Phys. **60**, 186–196 (2004).

[7]Y. Nagata, K. Takayama, Y. Matsuo, Y. Norihisa, T. Mizowaki, T. Sakamoto, M. Sakamoto, M. Mitsumori, K. Shibuya, N. Araki, S. Yano, and M. Hiraoka, "Clinical outcomes of a phase I/II study of 48 Gy of stereotactic body radiotherapy in 4 fractions for primary lung cancer using a stereotactic body frame," Int. J. Radiat. Oncol., Biol., Phys. **63**, 1427–1431 (2005).

[8]L. Potters, M. Steinberg, C. Rose, R. Timmerman, S. Ryu, J. M. Hevezi, J. Welsh, M. Mehta, D. A. Larson, and N. A. Janjan, "American Society for Therapeutic Radiology and Oncology and American College of Radiology practice guideline for the performance of stereotactic body radiation therapy," Int. J. Radiat. Oncol., Biol., Phys. **60**, 1026–1032 (2004).

[9]J. M. Balter, R. K. Ten Haken, T. S. Lawrence, K. L. Lam, and J. M. Robertson, "Uncertainties in CT-based radiation therapy treatment planning associated with patient breathing," Int. J. Radiat. Oncol., Biol., Phys. **36**, 167–174 (1996).

[10]S. Shimizu, H. Shirato, K. Kagei, T. Nishioka, X. Bo, H. Dosaka-Akita, S. Hashimoto, H. Aoyama, K. Tsuchiya, and K. Miyasaka, "Impact of respiratory movement on the computed tomographic images of small lung tumors in three-dimensional (3D) radiotherapy," Int. J. Radiat. Oncol., Biol., Phys. **46**, 1127–1133 (2000).

[11]G. T. Chen, J. H. Kung, and K. P. Beaudette, "Artifacts in computed tomography scanning of moving objects," Semin. Radiat. Oncol. **14**, 19–26 (2004).

[12]K. E. Rosenzweig, J. Hanley, D. Mah, G. Mageras, M. Hunt, S. Toner, C. Burman, C. C. Ling, B. Mychalczak, Z. Fuks, and S. A. Leibel, "The deep inspiration breath-hold technique in the treatment of inoperable non-small-cell lung cancer," Int. J. Radiat. Oncol., Biol., Phys. **48**, 81–87 (2000).

[13]D. Mah, J. Hanley, K. E. Rosenzweig, E. Yorke, L. Braban, C. C. Ling, S. A. Leibel, and G. Mageras, "Technical aspects of the deep inspiration breath-hold technique in the treatment of thoracic cancer," Int. J. Radiat. Oncol., Biol., Phys. **48**, 1175–1185 (2000).

[14]G. S. Mageras and E. Yorke, "Deep inspiration breath hold and respiratory gating strategies for reducing organ motion in radiation treatment," Semin. Radiat. Oncol. **14**, 65–75 (2004).

[15]F. J. Lagerwaard, J. R. van Sörnsen de Koste, M. R. Nijssen-Visser, R. H. Schuchhard-Schipper, S. S. Oei, A. Munne, and S. Senan, "Multiple "slow" CT scans for incorporating lung tumor mobility in radiotherapy planning," Int. J. Radiat. Oncol., Biol., Phys. **51**, 932–937 (2001).

[16]J. R. van Sörnsen de Koste, F. J. Lagerwaard, H. C. de Boer, M. R. Nijssen-Visser, and S. Senan, "Are multiple CT scans required for planning curative radiotherapy in lung tumors of the lower lobe?" Int. J. Radiat. Oncol., Biol., Phys. **55**, 1394–1399 (2003).

[17]J. R. van Sörnsen de Koste, F. J. Lagerwaard, M. R. Nijssen-Visser, W. J. Graveland, and S. Senan, "Tumor location cannot predict the mobility of lung tumors: a 3D analysis of data generated from multiple CT scans," Int. J. Radiat. Oncol., Biol., Phys. **56**, 348–354 (2003).

[18]E. C. Ford, G. S. Mageras, E. Yorke, and C. C. Ling, "Respiration-correlated spiral CT: a method of measuring respiratory-induced anatomic motion for radiation treatment planning," Med. Phys. **30**, 88–97 (2003).

[19]G. S. Mageras, A. Pevsner, E. D. Yorke, K. E. Rosenzweig, E. C. Ford, A. Hertanto, S. M. Larson, D. M. Lovelock, Y. E. Erdi, S. A. Nehmeh, J. L. Humm, and C. C. Ling, "Measurement of lung tumor motion using respiration-correlated CT," Int. J. Radiat. Oncol., Biol., Phys. **60**, 933–941 (2004).

[20]R. W. Underberg, F. J. Lagerwaard, J. P. Cuijpers, B. J. Slotman, J. R. van Sörnsen de Koste, and S. Senan, "Four-dimensional CT scans for treatment planning in stereotactic radiotherapy for stage I lung cancer," Int. J. Radiat. Oncol., Biol., Phys. **60**, 1283–1290 (2004).

[21]E. Rietzel, T. Pan, and G. T. Chen, "Four-dimensional computed tomography: Image formation and clinical protocol," Med. Phys. **32**, 874–889 (2005).

[22]E. Rietzel, A. K. Liu, K. P. Doppke, J. A. Wolfgang, A. B. Chen, G. T. Chen, and N. C. Choi, "Design of 4D treatment planning target volumes," Int. J. Radiat. Oncol., Biol., Phys. **66**, 287–295 (2006).

[23]Y. Negoro, Y. Nagata, T. Aoki, T. Mizowaki, N. Araki, K. Takayama, M. Kokubo, S. Yano, S. Koga, K. Sasai, Y. Shihamoto, and M. Hiraoka, "The effectiveness of an immobilization device in conformal radiotherapy for lung tumor: Reduction of respiratory tumor movement and evaluation of the daily setup accuracy," Int. J. Radiat. Oncol., Biol., Phys. **50**, 889–898 (2001).

[24]S. Seki, A. Takeda, T. Nagaoka, H. M. Deloar, T. Kawase, J. Fukuda, O. Kawaguchi, M. Uematsu, and A. Kubo, "Differences in the definition of internal target volumes using slow CT alone or in combination with thin-slice CT under breath-holding conditions during the planning of stereotactic radiotherapy for lung cancer," Radiother. Oncol. **85**, 443–449 (2007).

[25]J. D. Bradley, A. N. Nofal, I. M. El Naqa, W. Lu, J. Liu, J. Hubenschmidt, D. A. Low, R. E. Drzymala, and D. Khullar, "Comparison of helical, maximum intensity projection (MIP), and averaged intensity (AI) 4D CT imaging for steraotactic body radiation therapy (SBRT) planning in lung cancer," Radiother. Oncol. **81**, 264–268 (2006).

[26]B. Murray, K. Forster, and R. Timmerman, "Frame-based immobilization and targeting for stereotactic body radiation therapy," Med. Dosim. **32**, 86–91 (2007).

[27]S. Senan, J. van Sörnsen de Koste, M. Samson, H. Tankink, P. Jansen, P. J. Nowak, A. D. Krol, P. Schmitz, and F. J. Lagerwaard, "Evaluation of a target contouring protocol for 3D conformal radiotherapy in non-small cell lung cancer," Radiother. Oncol. **53**, 247–255 (1999).

[28]P. Bowden, R. Fisher, M. Mac Manus, A. Wirth, G. Duchesne, M. Millward, A. McKenzie, J. Andrews, and D. Ball, "Measurement of lung tumor volumes using three-dimensional computer planning software," Int. J. Radiat. Oncol., Biol., Phys. **53**, 566–573 (2002).

[29]Y. Matsuo, K. Takayama, Y. Nagata, E. Kunieda, K. Tateoka, N. Ishizuka, T. Mizowaki, Y. Norihisa, M. Sakamoto, Y. Narita, S. Ishikura, and M. Hiraoka, "Interinstitutional variations in planning for stereotactic body radiation therapy for lung cancer," Int. J. Radiat. Oncol., Biol., Phys. **68**, 416–425 (2007).

[30]Y. Seppenwoolde, H. Shirato, K. Kitamura, S. Shimizu, M. Van Herk, J. V. Lebesgue, and K. Miyasaka, "Precise and real-time measurement of 3D tumor motion in lung due to breathing and heartbeat, measured during radiotherapy," Int. J. Radiat. Oncol., Biol., Phys. **53**, 822–834 (2002).

[31]C. Plathow, S. Ley, C. Fink, M. Puderbach, W. Hosch, A. Schmähl, J. Debus, and H. U. Kauczor, "Analysis of intrathoracic tumor mobility during whole breathing cycle by dynamic MRI," Int. J. Radiat. Oncol., Biol., Phys. **59**, 952–959 (2004).

[32]Q. S. Chen, M. S. Weinhous, F. C. Deibel, J. P. Ciezki, and R. M. Macklis, "Fluoroscopic study of tumor motion due to breathing: Facilitating precise radiation therapy for lung cancer patients," Med. Phys. **28**, 1850–1856 (2001).

[33]K. Takayama, Y. Nagata, Y. Negoro, T. Mizowaki, T. Sakamoto, M. Sakamoto, T. Aoki, S. Yano, S. Koga, and M. Hiraoka, "Treatment planning of stereotactic radiotherapy for solitary lung tumor," Int. J. Radiat. Oncol., Biol., Phys. **61**, 1565–1571 (2005).

Development of a three-dimensionally movable phantom system for dosimetric verifications

Hiroshi Nakayama
Department of Radiation Oncology and Image-Applied Therapy, Graduate School of Medicine, Kyoto University, 54 Shogoin-Kawaharacho, Sakyo-ku, Kyoto, 606-8507, Japan and Medical Systems Administration Office, Hiroshima Machinery Works, Mitsubishi Heavy Industries, Limited, 4-6-22, Kan-On-Shin-Machi, Nishi-Ku, Hiroshima, 733-8553, Japan

Takashi Mizowaki[a)] and Yuichiro Narita
Department of Radiation Oncology and Image-Applied Therapy, Graduate School of Medicine, Kyoto University, 54 Shogoin-Kawaharacho, Sakyo-ku, Kyoto, 606-8507, Japan

Noriyuki Kawada, Kunio Takahashi, and Kazumasa Mihara
Medical Systems Administration Office, Hiroshima Machinery Works, Mitsubishi Heavy Industries, Limited, 4-6-22, Kan-On-Shin-Machi, Nishi-Ku, Hiroshima, 733-8553, Japan

Masahiro Hiraoka
Department of Radiation Oncology and Image-Applied Therapy, Graduate School of Medicine, Kyoto University, 54 Shogoin-Kawaharacho, Sakyo-ku, Kyoto, 606-8507, Japan

(Received 30 August 2007; revised 19 February 2008; accepted for publication 19 February 2008; published 7 April 2008)

The authors developed a three-dimensionally movable phantom system (3D movable phantom system) which can reproduce three-dimensional movements to experimentally verify the impact of radiotherapy treatment-related movements on dose distribution. The phantom system consists of three integrated components: a three-dimensional driving mechanism (3D driving mechanism), computer control system, and phantoms for film dosimetry. The 3D driving mechanism is a quintessential part of this system. It is composed of three linear-motion tables (single-axis robots) which are joined orthogonally to each other. This mechanism has a motion range of 100 mm, with a maximum velocity of 200 mm/s in each dimension, and 3D motion ability of arbitrary patterns. These attributes are sufficient to reproduce almost all organ movements. The positional accuracy of this 3D movable phantom system in a state of geostationary is less than 0.1 mm. The maximum error in terms of the absolute position on movement was 0.56 mm. The positional reappearance error on movement was up to 0.23 mm. The observed fluctuation of time was 0.012 s in the cycle of 4.5 s of oscillation. These results suggested that the 3D movable phantom system exhibited a sufficient level of accuracy in terms of geometry and timing to reproduce interfractional organ movement or setup errors in order to assess the influence of these errors on high-precision radiotherapy such as stereotactic irradiation and intensity-modulated radiotherapy. In addition, the authors 3D movable phantom system will also be useful in evaluating the adequacy and efficacy of new treatment techniques such as gating or tracking radiotherapy. [DOI: 10.1118/1.2897971]

Key words: organ motion, simulation, quality assurance, radiation therapy

I. INTRODUCTION

Recently, high-precision radiotherapy, such as stereotactic irradiation and intensity-modulated radiotherapy (IMRT), has become widely applied in routine clinical practices throughout the world. With these techniques, the delivery of excellent dose concentrations to targets and the sparing of organs at risk (OARs) can be achievable along with a steep dose gradient around the targets. Furthermore, in IMRT, nonuniform photon fluence in a field is achieved by changing field shapes as the irradiation time elapses.[1,2] Because of the features of high-precision radiotherapy described above, it is expected that treatment-related errors such as setup errors and the errors occurred by internal organ movements can lead to a much larger impact on the dose actually delivered to the targets and OARs compared to traditional irradiation techniques with relatively larger margins and uniform beam fluence in each radiation field. In other words, even a slight positional divergence of targets or OARs from a planned position causes large differences between planned and actually delivered dose distributions.[3–5] The existing software commercially available for radiotherapy treatment planning (RTP), however, cannot take into account such uncertainties in planning treatment and calculating dose. Treatment plans therefore are currently created using an image data set of static computed tomography (CT) scans as a standard clinical practice and evaluated based on the presumption that objects do not move at all, and only static dose distributions are measured by chamber or film dosimetry for quality assurance of IMRT.[6,7] To overcome the above-described problems, a few movable phantom systems, which facilitate the evalua-

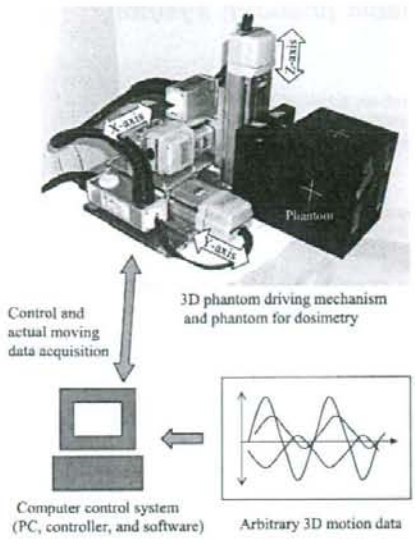

FIG. 1. 3D movable phantom system. The photo shows the 3D driving mechanism and attached dosimetric phantom.

tion of impacts on treatment-related errors of dose distribution, have been introduced.[8–10] These systems, however, have not been able to completely realize the arbitrary three-dimensional (3D) movements.[8–10] Other systems, which reproduce arbitrary movements have been developed, however, no system of them has been achieved the sufficient positional accuracy for the quality assurance of IMRT under the condition of driving a heavy dosimetric phantom.[11–13] We therefore developed the 3D movable phantom system that can load heavy dosimetric phantoms and accurately simulate arbitrary 3D movements. In the present article, details of the phantom system are described, and the accuracy of the system in simulating 3D movements is evaluated.

II. MATERIALS AND METHODS

II.A. 3D movable phantom system

II.A.1. System overview

The 3D movable phantom system is designed to fit linear accelerators or CT. This system consists of the following three components: a 3D driving mechanism, a computers control system, and phantoms for film dosimetry. Configurations of the system are indicated in Fig. 1.

II.A.2. 3D phantom driving mechanism

The 3D driving mechanism is composed of a phantom support base and three linear actuators along with three different axes, those are called single-axis robots. The single-axis robot is a device with a slider that can move on a linear guide fixed to the outer frame. The slider is able to move arbitrarily on the linear guide by a ball-screw mechanism. The first single-axis robot is fixed to an iron base plate in a direction whereby the slider of the robot is able to move, along the cephalocaudal axis (Y axis). This robot is called the Y-axis robot. The second robot, which is called the X-axis robot, is fixed to the slider of the Y-axis robot, and the slider of the X-axis robot can move in a left-and-right direction (X axis). The third and last robot, called the Z-axis robot, is fixed to the slider of the X-axis robot and can move parallel to the vertical direction (Z axis). The support base for the phantoms is mounted on the slider of the Z-axis robot (Fig. 1). The X- and Y-axis robots are ISA-SXM-1-60-4-100-T1-AQ (IAI Corp., Shizuoka, Japan), and the Z-axis robot is ISA-SXM-1-60-4-100-T1-AQ-B-NM (IAI Corp., Shizuoka, Japan), which is a model added a braking mechanism to the foregoing. Details of the performance specifications of these robots are indicated in Table I.[27] The dimensions of the 3D driving mechanism with the iron base plate are: 41, 34, and 38 cm in width (X axially), length (Y axially), and height (Z axially), respectively. The total weight is 23.6 kg.

II.A.3. Computers control system

The 3D driving mechanism is composed only of mechanical parts except for a positional sensor and a driving motor.

TABLE I. Performance specification of the single-axis robot.

Model		ISA-SXM-1-60-4-100-T1-AQ or ISA-SXM-1-60-4-100-T1-AQ-B-NM
Movable range		100 mm
Maximum acceleration	Horizontal	0.5 G (1.0 G=9800 mm/s^2)
	Vertical	0.3 G (1.0 G=9800 mm/s^2)
Load-bearing capacity	Horizontal	30 kg
	Vertical	12 kg
Maximum speed		200 mm/s
Repetition positioning accuracy		±0.02 mm
Drive system		12 mm diameter ball screw (rolled thread C10)
Backlash		0.05 mm or less
Usable temperature range		From 0 to 40 °C

Radiation-sensitive electric circuits such as microprocessors for controlling are separated and attached to a multiaxis controller (XSEL-K-3-601-601-601 B-N1-N1N2N2-2-1) (IAI Corp., Shizuoka, Japan). This controller instructs each robot of the 3D driving mechanism to perform individual arbitrary movements. The directed data of the 3D motion are represented by the movement of the three axes of X, Y, and Z, which is constructed on a personal computer and transferred to the controller beforehand. The 3D movable phantom system then achieves the reproduction of arbitrary movements by controlling the 3D driving mechanism using this data. The 3D driving mechanism is connected to the multiaxis controller with cables of 10 m in length, so that the 3D driving mechanism can be operated in a radiation field by remote control. Additionally, the multiaxis controller can read out value of the movement of each single-axis robot by directing the value of the internal sensor of the robot, which continuously monitors the position of the slider of each single-axis robot. The resolution in reading the value of movement by the controller was 0.1 mm, and the accuracy of the sensor in detecting positions was 0.02 mm or less.[27] In this study, output values by this sensor were recorded as "output value measured by the internal sensor."

II.A.4. Phantoms for film dosimetry

We designed two types of phantoms. One is a cubic phantom of 17 cm on each side, which a square-shaped dosimetric film of 14 cm by 14 cm can be inserted inside. The weight of the phantom is 5.2 kg. The other one is a spherical phantom with a diameter of 19 cm, in which a square-shaped film of 14 cm by 14 cm can be placed. The weight is 3.8 kg. Both of them are made from black ABS resin with a density of 1.05, which can effectively shield the film placed in the phantom from external light. The configurations of the phantoms are shown in Fig. 2.

II.B. Verification of the accuracy of the phantom system

Polaris Vicra system (Northern Digital, Inc., Ontario, Canada) was used as an independent verification system of the phantom position. The system consists of two major components. One is a position sensor unit that emits infrared light and tracks the position of the target object. The other one is a passive infrared marker, which is attached to the target object and recognized by the position sensor unit. The absolute accuracy of the position sensor unit is 0.25 mm or less, and its reproduction accuracy is 0.2 mm or less. In this study, the output value from the Polaris Vicra system was recorded as "the output value measured by the external monitor." This system was applied to the verification studies for both positional accuracy in the static condition and reproducibility of sinusoidal motion.

II.B.1. Positional accuracy in the static condition

To confirm the mechanical accuracy of the 3D movable phantom system, the positional accuracy in the step-by-step motion of the phantom system was verified. A program to command the 3D driving mechanism to move the phantom support base between 27 points one by one in 3D was created. At each measurement point, the output values measured by the external monitor and the values by the internal sensor were compared with the directed values by corresponding program. The program of the step-by step motion was executed using two patterns. One had a step size of 30 mm, as shown in Fig. 3 and the other one, 50 mm. Each pattern of movement was performed three times with respect to the

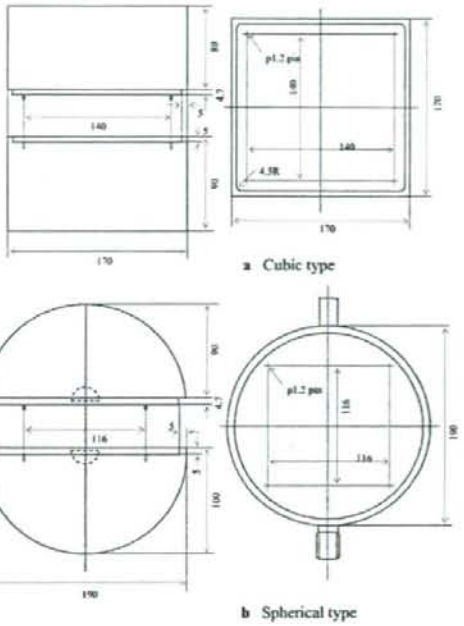

FIG. 2. Dosimetric phantoms. Technical drawings of the dosimetric phantoms. The cubic type of phantom is shown in the photograph of Fig. 1.

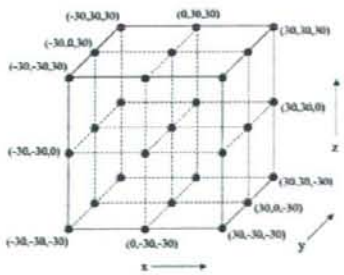

FIG. 3. Points for verification of the positional accuracy in the static condition. This figure shows the coordinates of 27 points that were used in the test for static positional accuracy, indicated by black dots. Each point was arranged with an interval of 30 mm in this example.

TABLE II. Outline of respiratory wave form data.

Frequency	4.5 s per one cycle (0.222 Hz)
Amplitude	X: 4.4 mm, Y: 5.735 mm, Z: 4.388 mm
Amount of data	69 points every 120 ms (2 cycles, 9 s of data)

following two different scenarios: in one scenario, only a phantom support base was driven, while in the other scenario, a globular phantom of 3.8 kg attached to the base was driven.

II.B.2. Reproducibility of sinusoidal motion

A data set of sinusoidal motion with a 30 mm peak-to-peak amplitude and a cycle time of 4.0022 s was created as directional data by piecewise linear approximation from an ideal sine wave form. Then, the 3D driving mechanism attached the globular phantom was operated to reproduce 30 cycles of sinusoidal motion of the three single-axis robots concurrently. During the 30 cycles of motion, the time course of the measured output values both by the external monitor and the internal sensor was recorded. To verify the accuracy in terms of the time course of this 3D movable phantom system, the length of each cycle for phantom motion was calculated from the time required for 30 cycles of movement and the peak-to-peak amplitude of the phantom motion was calculated from the 30 cycles of oscillations. These operations were executed with respect to each output values. In addition, the absolute accuracy of a wave form and its reproducibility were evaluated. The coordinates for two wave form cycles were extracted from the output values by both the external monitor and the internal sensor. Then, the output data from both the external monitor and the internal sensor were compared with the corresponding directed values and the differences were calculated, as the error of the absolute accuracy of a wave form. Furthermore, the averaged wave form of 30 cycles was calculated and the differences from averaged wave form to each of the 30 wave forms were calculated as the error of wave form reproducibility.

II.B.3. Reproducibility of respiratory motion

Here we verified whether the system could mechanically reproduce the cycles of the actual respiratory motion. The 3D coordinates of two cycles of respiratory oscillations of a tumor position obtained from the fluoroscopic image of a patient with lung cancer were used to create the wave form data for direction. An outline of the data is shown in Table II. The 3D driving mechanism loaded the globular phantom was operated according to that data. During 12 cycles of respiratory motion, the output values by the internal sensors were continuously recorded, then the cycle length and the peak-to-peak amplitude of the movement were calculated from the output values. The deviation between the output values and the direction of motion was calculated as the error of the absolute accuracy of the wave form. Next, the accuracy of wave form reproduction was evaluated by repeatedly operating the 3D driving mechanism five times. The averaged values of the measured coordinates were computed from the five data sets of the coordinates from those operations. The differences between the averaged values and each actual value of the coordinates were calculated as the error of wave-form reproducibility.

III. RESULTS

III.A. Positional accuracy in the static condition

A summary of the positional accuracy in the static condition measured by the external monitor is shown in Table III. There were only small differences of 0.1 mm or less between the directed values and the values measured by the external monitor with a very small number of dispersion. Moreover, there were no detectable differences between the directed values and the output values measured by the internal sensor (data are not shown). The results were the same even though a phantom of 3.8 kg in weight was attached to the driving mechanism.

III.B. Reproducibility of sinusoidal motion

The mean value of the cycle length was 4.01 s, and significant standard deviation (SD) value could not be calculated because the deviation was very small. Both outputs derived the same value associated with time.

A summary of the verification of geometrical reproducibility of sinusoidal motion is shown in Table IV. The maximum deflection of the amplitude was 0.08 mm by the external monitor and 0.2 mm by the internal sensor, respectively. The mean value and SD of the measured amplitude were 30.05 and 0.005 mm by the external monitor and 29.9 and 0.008 mm by the internal sensor; respectively. The maximum error and mean value of the error on the absolute accuracy of the motion trajectory measured by the external monitor were 0.18 and 0.053 mm, respectively. These errors measured by the internal sensor were 0.247 and 0.064 mm, respectively. The maximum error and mean value of the error on the wave form reproducibility measured by the external monitor was 0.121 and 0.027 mm, respectively. These errors measured by the internal sensor were 0.198 and 0.063 mm, respectively. Figure 4 indicates the relation between the directed values and the measured values that related to the movement of the phantom. Data on two cycles of the sinusoidal wave form are shown in Fig. 4(a). The history of the deviation between the output values and the corresponding directed value is indicated in Fig. 4(b).

III.C. Reproducibility of respiratory motion

The value of the mean cycle length of the oscillation measured by the internal sensor was 4.498 s. The averaged time deviation from the directed value was 0.002 s, and the SD of the cycle length was 0.0122 s. Table V shows the results of comparison of the wave form between the directed value and the measured trajectory of the 3D driving mechanism on each coordinate. The maximum deviation of the amplitude

TABLE III. Positional accuracies in the static condition.

	Directed value			Mean of measurements by the external monitor			Deflection			Standard deviation (SD)		
Position number	x (mm)	y (mm)	z (mm)	x (mm)	y (mm)	z (mm)	x (mm)	y (mm)	z (mm)	x (mm)	y (mm)	z (mm)
1	0	0	0	0.00	0.00	0.00	0.00	0.00	0.00	0.000	0.000	0.000
2	0	0	−30	−0.01	−0.03	−30.00	−0.01	−0.03	0.00	0.003	0.007	0.002
3	0	30	−30	−0.01	30.03	−29.98	−0.01	0.03	0.02	0.002	0.007	0.010
4	30	30	−30	30.01	30.04	−30.00	0.01	0.04	0.00	0.003	0.010	0.012
5	30	0	−30	30.02	−0.01	−30.01	0.02	−0.01	−0.01	0.003	0.003	0.009
6	30	−30	−30	30.03	−30.06	−30.03	0.03	−0.06	−0.03	0.003	0.003	0.008
7	0	−30	−30	0.00	−30.07	−30.01	0.00	−0.07	−0.01	0.002	0.006	0.001
8	−30	−30	−30	−29.98	−30.05	−30.03	0.02	−0.05	−0.03	0.005	0.002	0.011
9	−30	0	−30	−29.99	−0.01	−30.01	0.01	−0.01	−0.01	0.008	0.007	0.010
10	−30	30	−30	−29.99	30.04	−29.99	0.01	0.04	0.01	0.007	0.004	0.014
11	0	30	0	−0.01	30.05	0.02	−0.01	0.05	0.02	0.003	0.010	0.014
12	30	30	0	30.02	30.05	−0.01	0.02	0.05	−0.01	0.003	0.014	0.008
13	30	0	0	30.02	0.00	−0.02	0.02	0.00	−0.02	0.002	0.007	0.014
14	30	−30	0	30.03	−30.04	−0.04	0.03	−0.04	−0.04	0.005	0.003	0.005
15	0	−30	0	0.01	−30.05	−0.03	0.01	−0.05	−0.03	0.004	0.007	0.007
16	−30	−30	0	−29.99	−30.04	−0.04	0.01	−0.04	−0.04	0.006	0.010	0.007
17	−30	0	0	−29.99	0.01	−0.02	0.01	0.01	−0.02	0.005	0.008	0.010
18	−30	30	0	−29.99	30.07	0.00	0.01	0.07	0.00	0.008	0.015	0.011
19	0	30	30	0.00	30.09	30.00	0.00	0.09	0.00	0.003	0.005	0.017
20	30	30	30	30.01	30.07	29.99	0.01	0.07	−0.01	0.003	0.016	0.012
21	30	0	30	30.01	0.01	29.98	0.01	0.01	−0.02	0.002	0.007	0.014
22	30	−30	30	30.03	−30.04	29.96	0.03	−0.04	−0.04	0.005	0.010	0.015
23	0	−30	30	0.00	−30.03	29.98	0.00	−0.03	−0.02	0.006	0.006	0.010
24	−30	−30	30	−29.99	−30.03	29.96	0.01	−0.03	−0.04	0.006	0.008	0.010
25	−30	0	30	−30.00	0.02	29.98	0.00	0.02	−0.02	0.004	0.017	0.011
26	−30	30	30	−30.00	30.09	30.00	0.00	0.09	0.00	0.009	0.014	0.013
27	0	0	30	0.00	0.03	29.99	0.00	0.03	−0.01	0.003	0.010	0.007

and SD were 0.088 and 0 mm, respectively. The maximum deflection of the directed value and the measured value representing the absolute accuracy of the wave form was 0.56, and the SD was 0.12 mm. Figure 5(a) indicates an example of the correlation between the directed value and the measured value. Figure 5(b) shows the history of deviation between the measured value and corresponding directed value. The maximum deflection of the reproducibility of the wave form was 0.22 mm, with a SD value of 0.039 mm. Figure 6(a) shows an instance of the correlation between the mean value of the measurements and the value of one measurement, which indicates the reproducibility of the wave form. Figure 6(b) represents the difference between the mean value of the measurements and one of the measurements.

TABLE IV. Positional accuracy on sinusoidal movement.

				Error of absolute accuracy		Error of wave form reproducibility	
	Axis of oscillation	Maximum deflection of amplitude (mm)	Mean of amplitude (mm)	Maximum deflection (mm)	Mean of deflection (mm)	Maximum deflection (mm)	Mean of deflection (mm)
Measured with external monitor	X	0.080(SD=0.031)	30.03(SD=0.005)	0.162	0.035	0.093	0.022
	Y	0.065(SD=0.034)	30.05(SD=0.003)	0.157	0.036	0.092	0.023
	Z	0.070(SD=0.035)	30.02(SD=0.003)	0.180	0.053	0.121	0.027
Measured with internal sensor	X	0.00(SD=0.00)	30.0(SD=0.000)	0.219	0.060	0.16	0.044
	Y	0.00(SD=0.00)	30.0(SD=0.000)	0.247	0.062	0.198	0.048
	Z	0.20(SD=0.011)	29.9(SD=0.008)	0.247	0.064	0.184	0.063